

$\gamma\gamma \rightarrow t\bar{c} + c\bar{t}$ in a supersymmetric theory with an explicit R-parity violation *

Yu Zeng-Hui ^{a,c} Herbert Pietschmann ^a Ma Wen-Gan ^{b,c} Han Liang ^c Jiang Yi ^c

^aInstitut für Theoretische Physik, Universität Wien, A-1090 Vienna, Austria

^bCCAST (World Laboratory), P.O.Box 8730, Beijing 100080, P.R.China

^cDepartment of Modern Physics, University of Science and Technology
of China (USTC), Hefei, Anhui 230027, P.R.China

ABSTRACT

We studied the process $\gamma\gamma \rightarrow t\bar{c} + c\bar{t}$ in a R_p violating supersymmetric Model with the effects from both B- and L-violating interactions. The calculation shows that it is possible to detect a R_p violating signal at the Next Linear Collider. Information about the B-violating interaction in this model could be obtained under very clean background, if we take the present upper bounds for the parameters in the supersymmetric R_p interactions. Even if we can not detect a signal of R_p in the experiment, we may get more stringent constraints on the heavy-flavor R_p couplings.

PACS number(s): 13.65.+i, 13.88.+e, 14.65.-q, 14.80.Dq, 14.80.Gt

*Supported in part by Committee of National Natural Science Foundation of China and Project IV.B.12 of scientific and technological cooperation agreement between China and Austria

I. Introduction

The minimal supersymmetric model (MSSM)[1] is one of the most interesting extensions of the Standard Model (SM). It is considered as the most favorable model beyond SM. Thus it is interesting to confirm whether R-parity(R_p), a discrete multiplicative symmetry, is conserved in the supersymmetric extension of the SM. Because of the lack of credible theoretical arguments and experimental tests for R_p conservation, we can say that the R_p violation (R_p) would be equally well motivated in the supersymmetric extension of the SM. Even if we do not find a direct signal of MSSM, it would be a significant result to obtain a signal on R_p violation, which has recently motivated some investigations[2][3][4] because of experimentally observed discrepancies.

In the last few years, many efforts were made to find R_p interactions in experiments. Unfortunately, up to now we have only some upper limits on R_p parameters, such as B-violating R_p parameters (λ'') and L-violating R_p parameters(λ and λ')[4][5][6] (The parameters will be defined clearly in the following sector). Therefore, trying to find the signal of R_p violation or getting more stringent constraints on the parameters in future experiments, is a promising task. The popular way to find a R_p violation signal is to detect the decay of the lightest supersymmetric particle(LSP)[4] [6][7].

Recently S. Bar-Shalom et.al studied $\tilde{\nu} \rightarrow \gamma\gamma$ in hadron and photon collisions[8], they present a possible way to detect the R_p parameters λ' . In another work[9], they considered the decays $t \rightarrow c\tilde{\nu}$ and $\tilde{\nu} \rightarrow t\bar{c}$, in which there is supersymmetric particle number violation. There is another way to consider indirect effects of supersymmetric

particle number violation in the process $e^+e^- \rightarrow \gamma\gamma \rightarrow t\bar{c} + c\bar{t}$ in the future Next Linear Collider(NLC). This rare process can be used to get indirect information on R_p . Although small values of λ' and λ'' in R_p theory would suppress this process, the present upper bounds on R_p parameters just admit experimental observation ($O(\lambda')$ and $O(\lambda'')$ can be of order 1 when they involve heavy flavors). So we can hope this process allows detection of R_p violation within the present parameter upper limits. In the Standard Model, the process $\gamma\gamma \rightarrow t\bar{c} + c\bar{t}$ is suppressed by the GIM mechanism. So we can neglect the background of the SM as long as R_p parameters are close to present upper bounds.

With the advent of new collider techniques, we can produce highly coherent laser beams being back-scattered with high luminosity and efficiency at the e^+e^- colliders.[10] The $\gamma\gamma$ collisions give us a very clean environment to study the $t\bar{c}$ (or $c\bar{t}$) production. Effects of L-violating parameters in the e^+e^- collisions have been studied[4][6][8], but only little attention was paid to B-violating parameters[11]. The process considered here, can give us a chance to detect *B – violating* parameters λ'' in a very *clean* environment. We can also get information on the parameter λ' from the process, especially for heavy flavors, which are only weakly constrained by present data.

Because other flavor-changing mechanisms[12] beyond the SM can also be introduced in the $t\bar{c}$ (or $c\bar{t}$) production from $\gamma\gamma$ collisions, there would be some trouble in distinguishing these models, if the R_p interaction is not strong enough. But it may give us a chance to compare those models with R_p supersymmetric model; even when we can't find a clear signal of R_p , we can get estimations of background for other models.

In this work we concentrate on the the process $e^+e^- \rightarrow \gamma\gamma \rightarrow t\bar{c} + c\bar{t}$ in the R-parity violating supersymmetric theory. In section 2, we give the supersymmetric \mathcal{R}_p interactions. In section 3 we give the analytical calculations of $\gamma\gamma \rightarrow t\bar{c} + c\bar{t}$. In section 4 the numerical results of the process $e^+e^- \rightarrow \gamma\gamma \rightarrow t\bar{c} + c\bar{t}$ are presented. The conclusion is given in section 5 and some details of the expressions are listed in the appendix.

II. R-parity violation(\mathcal{R}_p) in MSSM

All renormalizable supersymmetric \mathcal{R}_p interactions can be introduced in the superpotential[4]:

$$W_{\mathcal{R}_p} = \frac{1}{2}\lambda_{[ij]k}L_i.L_j\bar{E}_k + \lambda'_{ijk}L_i.Q_j\bar{D}_k + \frac{1}{2}\lambda''_{[jk]i}\bar{U}_i\bar{D}_j\bar{D}_k + \epsilon_i L_i H_u. \quad (2.1)$$

where L_i , Q_i and H_u are SU(2) doublets containing lepton, quark and Higgs superfields respectively, \bar{E}_j (\bar{D}_j , \bar{U}_j) are the singlets of lepton (down-quark and up-quark), and i, j, k are generation indices and square brackets on them denote antisymmetry in the bracketed indices.

We ignored the last term in Eq(2.1) because its effects are rather small in our process[4][13]. So we have 9 λ -type, 27 λ' -type and 9 λ'' -type independent parameters left. The Lagrangian density of \mathcal{R}_p is given as follows:

$$L_{\mathcal{R}_p} = L_{\mathcal{R}_p}^\lambda + L_{\mathcal{R}_p}^{\lambda'} + L_{\mathcal{R}_p}^{\lambda''} \quad (2.2)$$

$$L_{\mathcal{R}_p}^\lambda = \lambda_{[ij]k}[\tilde{\nu}_{iL}\bar{e}_{kR}e_{jL} + \tilde{e}_{jL}\bar{e}_{kR}\nu_{iL} + \tilde{e}_{kR}^*\bar{\nu}_{iL}^C e_{jL} - \tilde{\nu}_{jL}\bar{e}_{kR}e_{iL} - \tilde{e}_{iL}\bar{e}_{kR}\nu_{jL} - \tilde{e}_{kR}^*\bar{\nu}_{jL}^C e_{iL}] + h.c.$$

$$L_{\not{R}_p}^{\lambda'} = \lambda'_{ijk} [\tilde{\nu}_{iL} \bar{d}_{kR} d_{jL} + \tilde{d}_{jL} \bar{d}_{kR}^C \nu_{iL} + \tilde{d}_{kR}^* \bar{\nu}_{iL}^C d_{jL} - \tilde{e}_{iL} \bar{d}_{kR} u_{jL} - \tilde{u}_{jL} \bar{d}_{kR} e_{iL} - \tilde{d}_{kR}^* \bar{e}_{iL}^C u_{jL}] + h.c.$$

$$L_{\not{R}_p}^{\lambda''} = \lambda''_{i[jk]} \epsilon_{\alpha\beta\gamma} [\tilde{u}_{iR\alpha}^* \bar{d}_{kR\beta} d_{jR\gamma}^C + \tilde{d}_{jR\beta}^* \bar{u}_{iR\alpha} d_{kR\gamma}^C + \tilde{d}_{kR\gamma}^* \bar{u}_{iR\alpha} d_{jR\beta}^C] + h.c. \quad (2.3)$$

The proton lifetime suppresses the possibility of both B-violation and L-violation, leading to the constraints:[4]

$$|(\lambda \text{ or } \lambda')\lambda''| < 10^{-10} \left(\frac{\tilde{m}}{100 \text{ GeV}} \right)^2. \quad (2.4)$$

Therefore, we consider the contributions from $L_{\not{R}_p}^{\lambda'}$ and $L_{\not{R}_p}^{\lambda''}$ separately. Although the individual parameters λ , λ' and λ'' should be typically less than $10^{-1} - 10^{-2} \left(\frac{\tilde{m}}{100 \text{ GeV}} \right)^2$ [6], we can expect the parameters involving heavy flavors to be much larger in analogy with the Yukawa couplings in the MSSM[4]. Since the constraints on such parameters from present experimental data are rather weak, testing \not{R}_p at high energy is still very important.

III. Calculations

In the following calculations we assume the parameters λ' and λ'' to be real. One-loop corrections (as shown in Fig.1) of $\gamma(p_3)\gamma(p_4) \rightarrow t(p_1)\bar{c}(p_2)$ can be split into the following components:

$$M = \delta M_s + \delta M_v + \delta M_b. \quad (3.1)$$

where δM_s , δM_v and δM_b are the one-loop amplitudes corresponding to the self-energy, vertex, and box correction diagrams respectively. We find that amplitudes are proportional

to the products $\lambda'_{i2j}\lambda'_{i3j}$ ($i, j = 1, 2, 3$) (Fig.1.(a.1-2), Fig.1.(b.1-4) and Fig.1.(c.1-8)) and $\lambda''_{2ij}\lambda''_{3ij}$ ($i, j = 1, 2, 3$) (Fig.1.(a.3), Fig.1.(b.5-6) and Fig.1.(c.9-12)); thus it is possible to detect R_p signals or get much stronger constraints on those parameters by measuring this process in future NLC experiments.

We define the Mandelstam variables as usual

$$\hat{s} = (p_1 + p_2)^2 = (p_3 + p_4)^2 \quad (3.2)$$

$$\hat{t} = (p_1 - p_3)^2 = (p_4 - p_2)^2 \quad (3.2)$$

$$\hat{u} = (p_1 - p_4)^2 = (p_3 - p_2)^2 \quad (3.4)$$

The ultraviolet divergence is controlled by dimensional regularization ($n = 4 - \epsilon$) and renormalized by using on-mass-shell scheme. In the Appendix we will give the details of the amplitudes. Similarly, we can get the amplitude for subprocess $\gamma\gamma \rightarrow c\bar{t}$. Collecting all terms in Eq.(3.1), we obtain the total cross section for the subprocess $\gamma\gamma \rightarrow t\bar{c} + c\bar{t}$:

$$\hat{\sigma}(\hat{s}) = \frac{2N_c}{16\pi\hat{s}^2} \int_{\hat{t}^-}^{\hat{t}^+} d\hat{t} \sum_{spins} [|M|^2], \quad (3.5)$$

where $\hat{t}^\pm = \frac{1}{2} \left[(m_t^2 + m_c^2 - \hat{s}) \pm \sqrt{\hat{s}^2 + m_t^4 + m_c^4 - 2\hat{s} * m_t^2 - 2\hat{s} * m_c^2 - 2m_t^2 * m_c^2} \right]$, colour factor $N_c = 3$ and the bar over summation means averaging over initial spins. In order to get the observable results in the measurements of $t\bar{c} + \bar{t}c$ production via $\gamma\gamma$ fusion in e^+e^- collider, we need to fold the cross section of $\gamma\gamma \rightarrow t\bar{c} + c\bar{t}$ with the photon luminosity,

$$\sigma(s) = \int_{(m_t+m_c)/\sqrt{s}}^{x_{max}} dz \frac{dL_{\gamma\gamma}}{dz} \hat{\sigma}(\hat{s}), \quad (3.6)$$

where $\hat{s} = z^2 s$, \sqrt{s} and $\sqrt{\hat{s}}$ are the e^+e^- and $\gamma\gamma$ CMS energies respectively, and $\frac{dL_{\gamma\gamma}}{dz}$ is the photon luminosity, which is defined as[10]

$$\frac{dL_{\gamma\gamma}}{dz} = 2z \int_{z^2/x_{max}}^{x_{max}} \frac{dx}{x} F_{\gamma/e}(x) F_{\gamma/e}(z^2/x). \quad (3.7)$$

The energy spectrum of the back-scattered photon is given by [10].

$$F_{\gamma/e}(x) = \frac{1}{D(\xi)} \left[1 - x + \frac{1}{1-x} - \frac{4x}{\xi(1-x)} + \frac{4x^2}{\xi^2(1-x)^2} \right]. \quad (3.8)$$

taking the parameters of Ref.[14], we have $\xi = 4.8$, $x_{max} = 0.83$ and $D(\xi) = 1.8$.

IV. Numerical results

In the numerical calculations we assume $m_{\tilde{q}} = m_{\tilde{l}}$ and consider the effects from $L_{\tilde{R}_p}^{\lambda'}$ and $L_{\tilde{R}_p}^{\lambda''}$ separately.

For the B-violating parameter $\lambda_{2ij}'' \lambda_{3ij}'' (i, j = 1 - 3)$, upper bounds of λ_{223}'' and λ_{323}'' dominate all others, so we will neglect all other λ'' terms. For the L-violating parameter $\lambda_{i2j}' \lambda_{i3j}' (i, j = 1 - 3)$, we neglect all parameters except for λ_{323}' and λ_{333}' .

In Fig.2, we show the cross section of $e^+e^- \rightarrow \gamma\gamma \rightarrow t\bar{c} + c\bar{t}$ as function of c.m. energy of the electron-positron system at the upper bounds of λ'' , i.e. $\lambda_{323}'' \lambda_{223}'' = 0.625$, see Ref.[4]. We take $m_{\tilde{l}} = m_{\tilde{q}} = 100 \text{ GeV}$ (Solid line) and $m_{\tilde{l}} = m_{\tilde{q}} = 150 \text{ GeV}$ (Dashed line), respectively. The results show that the cross section can be 0.64 fb for solid line (0.29 fb for dashed line) when the c.m. energy (\sqrt{s}) is equal to 500 GeV. So if the electron-positron integrated luminosity of the NLC is 50 fb^{-1} , we can get about 32 events per year when

$m_{\tilde{l}} = m_{\tilde{q}} = 100 \text{ GeV}$. Therefore the R_p signal could be detected, if λ'' are large enough under the present allowed upper bounds.

In Fig.3, we plot the cross section of $e^+e^- \rightarrow \gamma\gamma \rightarrow t\bar{c} + c\bar{t}$ as function of c.m. energy of the electron-positron system with the upper bounds of λ' , i.e. $\lambda'_{333}\lambda'_{323} = 0.096$, see Ref.[4]. We take again $m_{\tilde{l}} = m_{\tilde{q}} = 100 \text{ GeV}$ for solid line and $m_{\tilde{l}} = m_{\tilde{q}} = 150 \text{ GeV}$ for dashed line, respectively. The cross section is much smaller than that of Fig.2. That looks reasonable because the upper limits of λ' from present data are much smaller than those of λ'' . The cross section can be only about 0.017 fb when $\sqrt{s} = 500 \text{ GeV}$, that means we can get only 1 event per year at the NLC with integrated luminosity 50 fb^{-1} . Thus it will be difficult to find the signal of λ' from the process which we discussed.

In order to give more stringent constraints of λ'' in future experiments, we draw the cross section at $\sqrt{s} = 500 \text{ GeV}$ as function of $\lambda''_{223}\lambda''_{323}$ in Fig.4(Solid line is for $m_{\tilde{l}} = m_{\tilde{q}} = 100 \text{ GeV}$ and dashed-line for $m_{\tilde{l}} = m_{\tilde{q}} = 150 \text{ GeV}$). When $\lambda''_{223}\lambda''_{323}$ is about 0.1, the cross section will be about 0.02 fb . That corresponds to 1 event per year at the NLC. So if we can't get the signal of R_p from the experiments, we can set the stronger constraint on λ''_{223} and λ''_{323} , i.e. $\lambda''_{223}\lambda''_{323} \leq 0.1$.

Similarly we draw the relation between the cross section and the parameter product $\lambda'_{323}\lambda'_{333}$ with $\sqrt{s} = 500 \text{ GeV}$ in Fig.5, solid line is for $m_{\tilde{l}} = m_{\tilde{q}} = 100 \text{ GeV}$ and dashed-line for $m_{\tilde{l}} = m_{\tilde{q}} = 150 \text{ GeV}$.

IV. Conclusion

We studied both the subprocess $\gamma\gamma \rightarrow t\bar{c} + c\bar{t}$ and process $e^+e^- \rightarrow \gamma\gamma \rightarrow t\bar{c} + c\bar{t}$ in one-loop order in explicit R_p supersymmetric model. The calculations show that we can test R_p theory in the future NLC experiments, if the B-violating couplings(λ'' -type) are large enough within the present experimentally admitted range. That means we can detect B-violating interactions in the lepton colliders with cleaner background. We also consider the effect from L-violating interactions (λ' -type), and conclude that it is very small in this process.

From our calculation, we find that the subprocess $\gamma\gamma \rightarrow t\bar{c} + c\bar{t}$ is very helpful in getting the information about the B-violating couplings(λ''). That is because the effect of L-violating interactions(λ') is small and can be neglected. Thus if we can observe events of this process in the NLC, we can conclude that they are from B-violation couplings. Even if we can't detect any signal from the experiments, we could improve the present upper bounds on $\lambda''_{223}\lambda''_{323}$.

Appendix

A. Loop integrals:

We adopt the definitions of two-, three-, four-point one-loop Passarino-Veltman integral functions of reference[15][16]. The integral functions are defined as follows:

1. The two-point integrals are:

$$\{B_0; B_\mu; B_{\mu\nu}\}(p, m_1, m_2) = \frac{(2\pi\mu)^{4-n}}{i\pi^2} \int d^n q \frac{\{1; q_\mu; q_\mu q_\nu\}}{[q^2 - m_1^2][(q+p)^2 - m_2^2]}, \quad (A.a.1)$$

The function B_μ should be proportional to p_μ :

$$B_\mu(p, m_1, m_2) = p_\mu B_1(p, m_1, m_2) \quad (A.a.2)$$

Similarly we get:

$$B_{\mu\nu} = p_\mu p_\nu B_{21} + g_{\mu\nu} B_{22} \quad (A.a.3)$$

We denote $\bar{B}_0 = B_0 - \Delta$, $\bar{B}_1 = B_1 + \frac{1}{2}\Delta$ and $\bar{B}_{21} = B_{21} - \frac{1}{3}\Delta$. with $\Delta = \frac{2}{\epsilon} - \gamma + \log(4\pi)$, $\epsilon = 4 - n$. μ is the scale parameter.

2. Three-point integrals:

$$\begin{aligned} & \{C_0; C_\mu; C_{\mu\nu}; C_{\mu\nu\rho}\}(p, k, m_1, m_2, m_3) = \\ & -\frac{(2\pi\mu)^{4-n}}{i\pi^2} \int d^n q \frac{\{1; q_\mu; q_\mu q_\nu; q_\mu q_\nu q_\rho\}}{[q^2 - m_1^2][(q+p)^2 - m_2^2][(q+p+k)^2 - m_3^2]}, \quad (A.a.4) \end{aligned}$$

We can change it to form-factors as follows:

$$C_\mu = p_\mu C_{11} + k_\mu C_{12}$$

$$\begin{aligned}
C_{\mu\nu} &= p_\mu p_\nu C_{21} + k_\mu k_\nu C_{22} + (p_\mu k_\nu + k_\mu p_\mu) C_{23} + g_{\mu\nu} C_{24} \\
C_{\mu\nu\rho} &= p_\mu p_\nu p_\rho C_{31} + k_\mu k_\nu k_\rho C_{32} + (k_\mu p_\nu p_\rho + p_\mu k_\nu p_\rho + p_\mu p_\nu k_\rho) C_{33} + \\
&\quad (k_\mu k_\nu p_\rho + p_\mu k_\nu k_\rho + k_\mu p_\nu k_\rho) C_{34} + (p_\mu g_{\nu\rho} + p_\nu g_{\mu\rho} + p_\rho g_{\mu\nu}) C_{35} + \\
&\quad (k_\mu g_{\nu\rho} + k_\nu g_{\mu\rho} + k_\rho g_{\mu\nu}) C_{36} \tag{A.a.5}
\end{aligned}$$

3. The four-point integrals:

$$\begin{aligned}
\{D_0; D_\mu; D_{\mu\nu}; D_{\mu\nu\rho}; D_{\mu\nu\rho\alpha}\}(p, k, l, m_1, m_2, m_3, m_4) = \\
\frac{(2\pi\mu)^{4-n}}{i\pi^2} \int d^n q \frac{\{1; q_\mu; q_\mu q_\nu; q_\mu q_\nu q_\rho; q_\mu q_\nu q_\rho q_\alpha\}}{[q^2 - m_1^2][(q+p)^2 - m_2^2][(q+p+k)^2 - m_3^2][(q+p+k+l)^2 - m_4^2]}, \tag{A.a.6}
\end{aligned}$$

Similarly we get form-factors of D functions:

$$\begin{aligned}
D_\mu &= p_\mu D_{11} + k_\mu D_{12} + l_\mu D_{13} \\
D_{\mu\nu} &= p_\mu p_\nu D_{21} + k_\mu k_\nu D_{22} + l_\mu l_\nu D_{23} + \{pk\}_{\mu\nu} D_{24} + \{pl\}_{\mu\nu} D_{25} + \{kl\}_{\mu\nu} D_{26} + g_{\mu\nu} D_{27} \\
D_{\mu\nu\rho} &= p_\mu p_\nu p_\rho D_{31} + k_\mu k_\nu k_\rho D_{32} + l_\mu l_\nu l_\rho D_{33} + \{kpp\}_{\mu\nu\rho} D_{34} + \\
&\quad \{lpp\}_{\mu\nu\rho} D_{35} + \{pkk\}_{\mu\nu\rho} D_{36} + \{pll\}_{\mu\nu\rho} D_{37} + \{lkk\}_{\mu\nu\rho} D_{38} + \\
&\quad \{kll\}_{\mu\nu\rho} D_{39} + \{pkl\}_{\mu\nu\rho} D_{310} + \{pg\}_{\mu\nu\rho} D_{311} + \{kg\}_{\mu\nu\rho} D_{312} + \{lg\}_{\mu\nu\rho} D_{313} \tag{A.a.7}
\end{aligned}$$

where

$$\{pk\}_{\mu\nu} = p_\mu k_\nu + k_\mu p_\nu$$

$$\{pkl\}_{\mu\nu\rho} = p_\mu k_\nu l_\rho + l_\mu p_\nu k_\rho + k_\mu l_\nu p_\rho$$

$$\{pg\}_{\mu\nu\rho} = p_\mu g_{\nu\rho} + p_\nu g_{\mu\rho} + p_\rho g_{\mu\nu} \quad (A.a.8)$$

The numerical calculation of the vector and tensor loop integral functions can be traced back to the four scalar loop integrals A_0 , B_0 , C_0 and D_0 in Ref.[15][16] and the references therein.

B. Self-energy part of the amplitude.

The amplitude of self-energy diagrams δM_s (Fig.1.(a)) can be decomposed into t-channel M_s^t and u-channel terms M_s^u . We will just give the expressions of t-channel, and u-channel can be obtained from t-channel, changing t into u and exchanging all indices and arguments of the incoming photons. The amplitude M_s^t can be expressed as:

$$\begin{aligned} \delta M_s^t = & \frac{-4\pi i \alpha Q_c Q_t}{(t - m_t^2)(t - m_c^2)} \epsilon^\mu(p_3) \epsilon^\nu(p_4) \bar{u}(p_1) \gamma_\mu \\ & (\not{p}_1 - \not{p}_3 + m_t) \left[\hat{\Sigma}(p_1 - p_3) \right] (\not{p}_1 - \not{p}_3 + m_c) \gamma_\nu v(p_2). \end{aligned} \quad (A.b.1)$$

where quark electric charge $Q_c = Q_t = 2/3$, $\alpha = 1/137.04$ and $\hat{\Sigma}(p)$ is defined as

$$-i\hat{\Sigma}(p) = H_L \not{p} P_L + H_R \not{p} P_R - H_L^S P_L - H_R^S P_R \delta_{kl}, \quad (A.b.2)$$

with

$$H_R = -i\Sigma_L + i\delta Z_L, \quad (A.b.3)$$

$$H_R = -i\Sigma_R + i\delta Z_R, \quad (A.b.4)$$

$$H_L^S = -i\delta M_L, \quad (A.b.5)$$

$$H_R^S = -i\delta M_R, \quad (A.b.6)$$

where

$$\Sigma_L = \frac{1}{16\pi^2} \lambda'_{i2j} \lambda'_{i3j} (B_1[-p, m_{q_j}, m_{\tilde{l}_i}] + B_1[-p, m_{l_i}, m_{\tilde{q}_j}]), \quad (A.b.7)$$

$$\Sigma_R = -\frac{IC_R}{16\pi^2} \lambda''_{2jk} \lambda''_{3jk} (B_1[-p, m_{q_j}, m_{\tilde{q}_k}] + B_1[-p, m_{q_k}, m_{\tilde{q}_j}]), \quad (A.b.8)$$

where i and j, k are generations of leptons and quarks respectively, $C_R = 2$ and the explicit expressions of the wave-function renormalization constants have the following forms:

$$\begin{aligned} \delta Z_L &= \frac{1}{m_t^2 - m_c^2} ((m_t \text{Re}[\Sigma_L]|_{p^2=m_t^2} + m_c \text{Re}[\Sigma_R]|_{p^2=m_c^2}) m_t \\ &\quad - (m_t \text{Re}[\Sigma_R]|_{p^2=m_t^2} + m_c \text{Re}[\Sigma_L]|_{p^2=m_c^2}) m_c), \end{aligned} \quad (A.b.9)$$

$$\begin{aligned} \delta Z_R &= \frac{1}{m_c^2 - m_t^2} ((m_t \text{Re}[\Sigma_L]|_{p^2=m_t^2} + m_c \text{Re}[\Sigma_R]|_{p^2=m_c^2}) m_c \\ &\quad - (m_t \text{Re}[\Sigma_R]|_{p^2=m_t^2} + m_c \text{Re}[\Sigma_L]|_{p^2=m_c^2}) m_t), \end{aligned} \quad (A.b.10)$$

$$\delta M_L = (\delta Z_R - \text{Re}[\Sigma_R]|_{p^2=m_c^2}) m_c, \quad (A.b.11)$$

$$\delta M_R = (\delta Z_L - \text{Re}[\Sigma_L]|_{p^2=m_c^2}) m_c. \quad (A.b.12)$$

3. The amplitude from vertex diagrams.

The amplitudes from vertex diagrams can be expressed as:

$$\delta M_v^{(l)} = \epsilon^\mu(p_3) \epsilon^\nu(p_4) \bar{u}(p_1) \Lambda^{(l)} v(p_2), \quad (l = t, u), \quad (A.c.1)$$

where

$$\begin{aligned} \Lambda^{(t)} &= \frac{eQ_c}{t - m_c^2} [\Lambda_\mu(p_1, p_3 - p_1)] (\not{p}_1 - \not{p}_3 + m_c) \gamma_\nu \\ &\quad + \frac{eQ_t}{t - m_t^2} \gamma_\mu (\not{p}_1 - \not{p}_3 + m_t) [\Lambda_\nu(p_4 - p_2, p_2)]. \end{aligned} \quad (A.c.2)$$

where $Q_t = Q_c = 2/3$, and $e^2 = 4\pi\alpha$. The $\gamma t\bar{c}$ vertex functions are composed of contributions from Fig.1.(b) and a counterterm, which is given by:

$$\Lambda_\mu^{(CT)} = -ieQ_t\gamma_\mu [\delta Z_L P_L + \delta Z_R P_R] \quad (A.c.3)$$

The wave function renormalization constants can be obtained from Eq.(A.b.9) and Eq.(A.b.10).

The box term can be obtained in a similar way from Fig.1.(c); however, it is very complex, so we omit to write it out explicitly. For a hint of its structure, compare Ref.[17]

References

- [1] H.E. Haber and G.L. Kane, Phys. Rep. **117**, 75(1985); J.F. Gunion and H.E. Haber, Nucl. Phys. **B272**, 1(1986).
- [2] S. Weinberg, Phys. Rev. D26(1982)287.
- [3] L.J. Hall and M. Suzuki, Nucl. Phys. B231(1984)419.
- [4] P. Roy, TIFR/TH/97-60; D.K. Ghosh, S. Raychaudhuri and K. Sridhar, Phys. Lett. B396(1997)177.
- [5] K. Agashe and M. Graesser, Phys. Rev. D54(1996)4445; J-H. Jiang, J.G. Kim and J.S. Lee, Phys. Rev. D55(1997)7296; Phys. Lett. B408(1997)367; Phys. Rev. D58(1998)035006.
- [6] G. Bhattacharyya, D. Choudhury and K. Sridhar, Phys. Lett. B355(1995)193; R. Barbier et.al, hep-ph/9810232.

- [7] D.K. Ghosh and S. Raychaudhuri, Phys. Lett. B422(1998)187.
- [8] S. Bar-Shalom, G. Eilam and J. Wudka, Phys.Rev.D59(1999)035010.
- [9] S. Bar-Shalom, G. Eilam and A. Soni, hep-ph/9812518.
- [10] V.Telnov, Nucl. Instrum. Meth. A294, 72(1990); L. Ginzburg, G. Kotkin and H. Spiesberger, Fortschr. Phys. 34, 687(1986).
- [11] D.K. Ghosh, R.M. Godbole and S. Raychaudhuri, Z. Phys. C75(1997)357.
- [12] D. Atwood et al. Phys. Rev. D53(1996)1199; W-S. Hou and G-L. Lin, Phys. Lett. B379(1996)261; Y. Jiang, M-l. Zhou, W-G. Ma, L. Han, H. Zhou and M. Han, Phys. Rev. D57(1998)4343.
- [13] R. Hempfling, Nucl. Phys. B478(1996)3; B. Mukhopadhyay and S. Roy, Phys. Rev. D55(1997)7020.
- [14] K.Cheung, Phys. Rev. D47(1993)3750; *ibid.* 50(1994)1173.
- [15] Bernd A. Kniehl, Phys. Rep. 240(1994)211.
- [16] G. Passarino and M. Veltman, Nucl. Phys. **B160**151(1979).
- [17] Z-H.Yu, H.Pietschmann, W-G.Ma, L.Han and Y.Jiang, hep-ph/9804331

Figure Captions

Fig.1 Feynman diagrams of $\gamma\gamma \rightarrow t\bar{c}$ subprocess. Fig.1 (a): Self-energy diagrams. Fig.1 (b): Vertex diagrams Fig.1 (c): Box diagrams (only t-channel). Dashed lines represent sleptons and squarks.

Fig.2 Cross section of $e^+e^- \rightarrow \gamma\gamma \rightarrow t\bar{c} + c\bar{t}$ as function of c.m.energy \sqrt{s} with $\lambda''_{323}\lambda''_{223} = 0.625$ solid line for $m_{\tilde{l}} = m_{\tilde{q}} = 100 \text{ GeV}$, and dashed line for $m_{\tilde{l}} = m_{\tilde{q}} = 150 \text{ GeV}$.

Fig.3 Cross section of $e^+e^- \rightarrow \gamma\gamma \rightarrow t\bar{c} + c\bar{t}$ as function of c.m.energy \sqrt{s} with $\lambda'_{333}\lambda'_{323} = 0.096$ solid line for $m_{\tilde{l}} = m_{\tilde{q}} = 100 \text{ GeV}$, and dashed line for $m_{\tilde{l}} = m_{\tilde{q}} = 150 \text{ GeV}$.

Fig.4 Cross section of $e^+e^- \rightarrow \gamma\gamma \rightarrow t\bar{c} + c\bar{t}$ at c.m.energy $\sqrt{s} = 500 \text{ GeV}$ as function of $\lambda''_{323}\lambda''_{223}$. solid line for $m_{\tilde{l}} = m_{\tilde{q}} = 100 \text{ GeV}$, and dashed line for $m_{\tilde{l}} = m_{\tilde{q}} = 150 \text{ GeV}$.

Fig.5 Cross section of $e^+e^- \rightarrow \gamma\gamma \rightarrow t\bar{c} + c\bar{t}$ at c.m.energy $\sqrt{s} = 500 \text{ GeV}$ as function of $\lambda'_{333}\lambda'_{323}$. solid line for $m_{\tilde{l}} = m_{\tilde{q}} = 100 \text{ GeV}$, and dashed line for $m_{\tilde{l}} = m_{\tilde{q}} = 150 \text{ GeV}$.

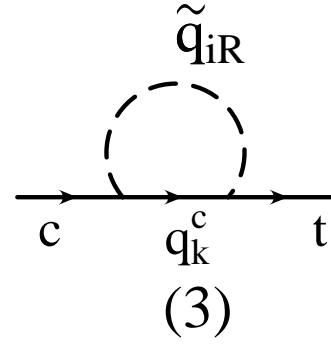
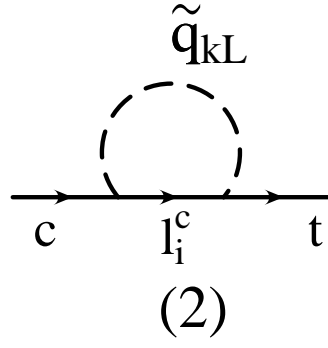
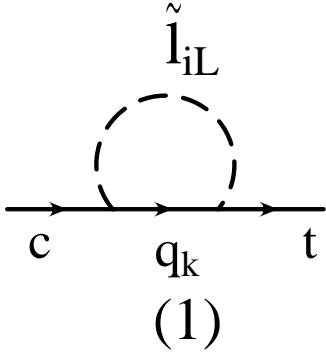


Fig.1 (a)

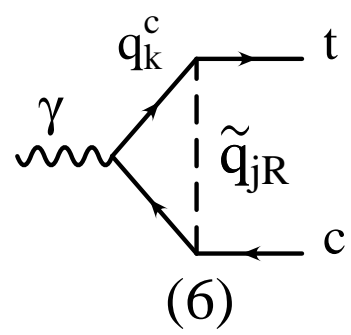
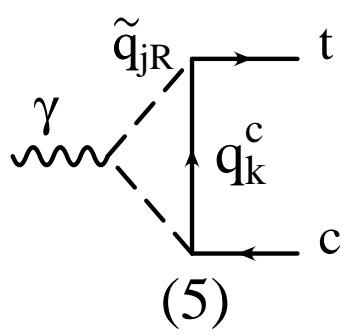
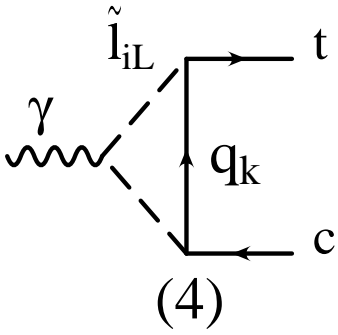
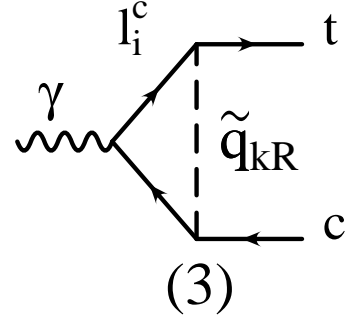
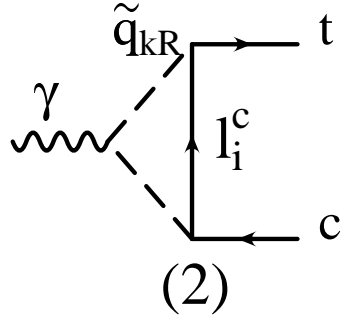
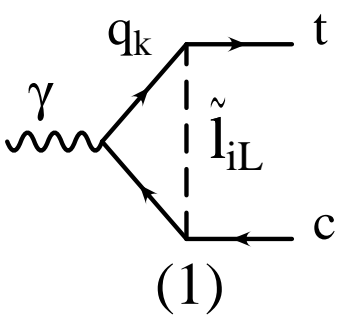


Fig.1 (b)

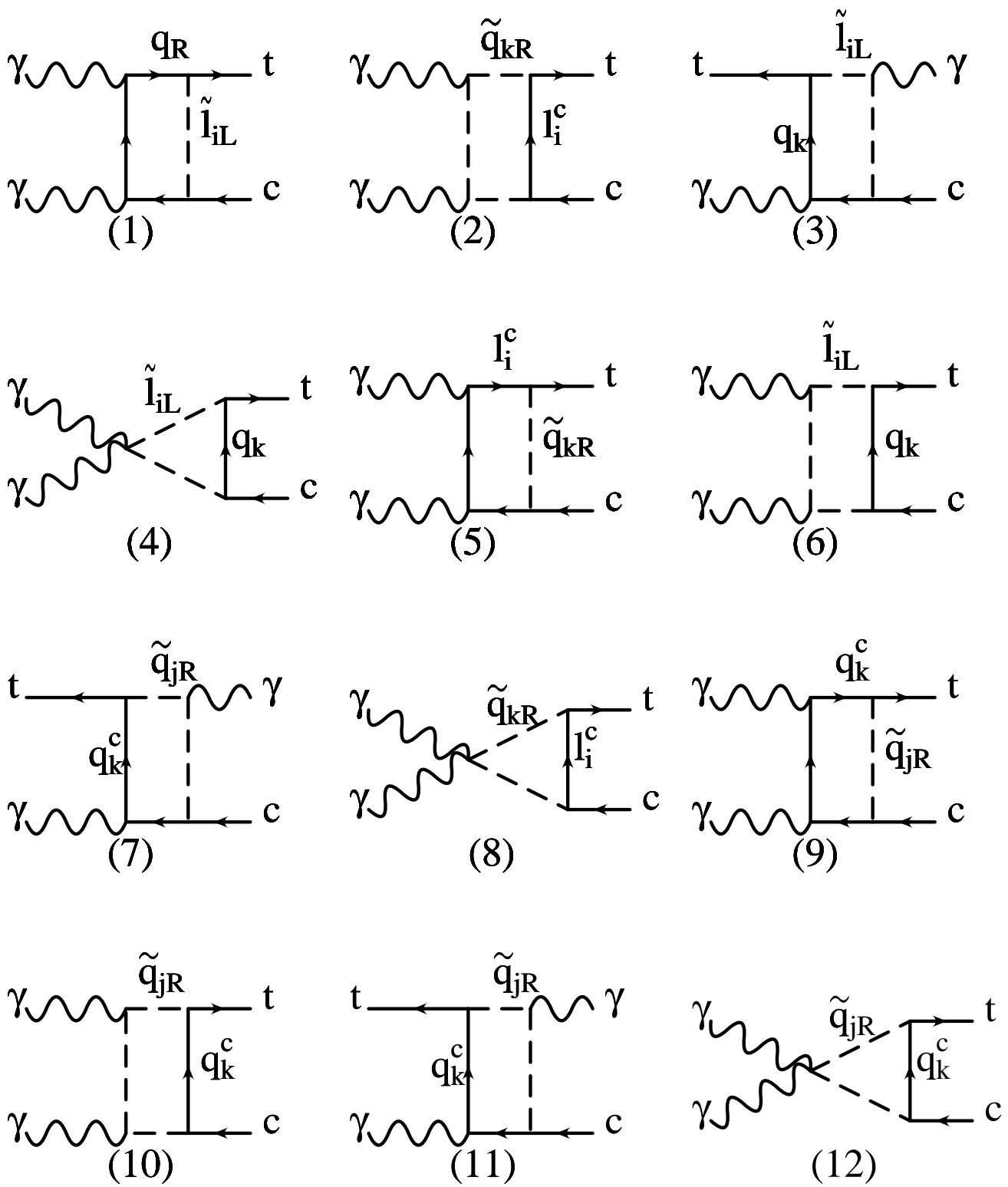


Fig.1 (c)

Fig.2

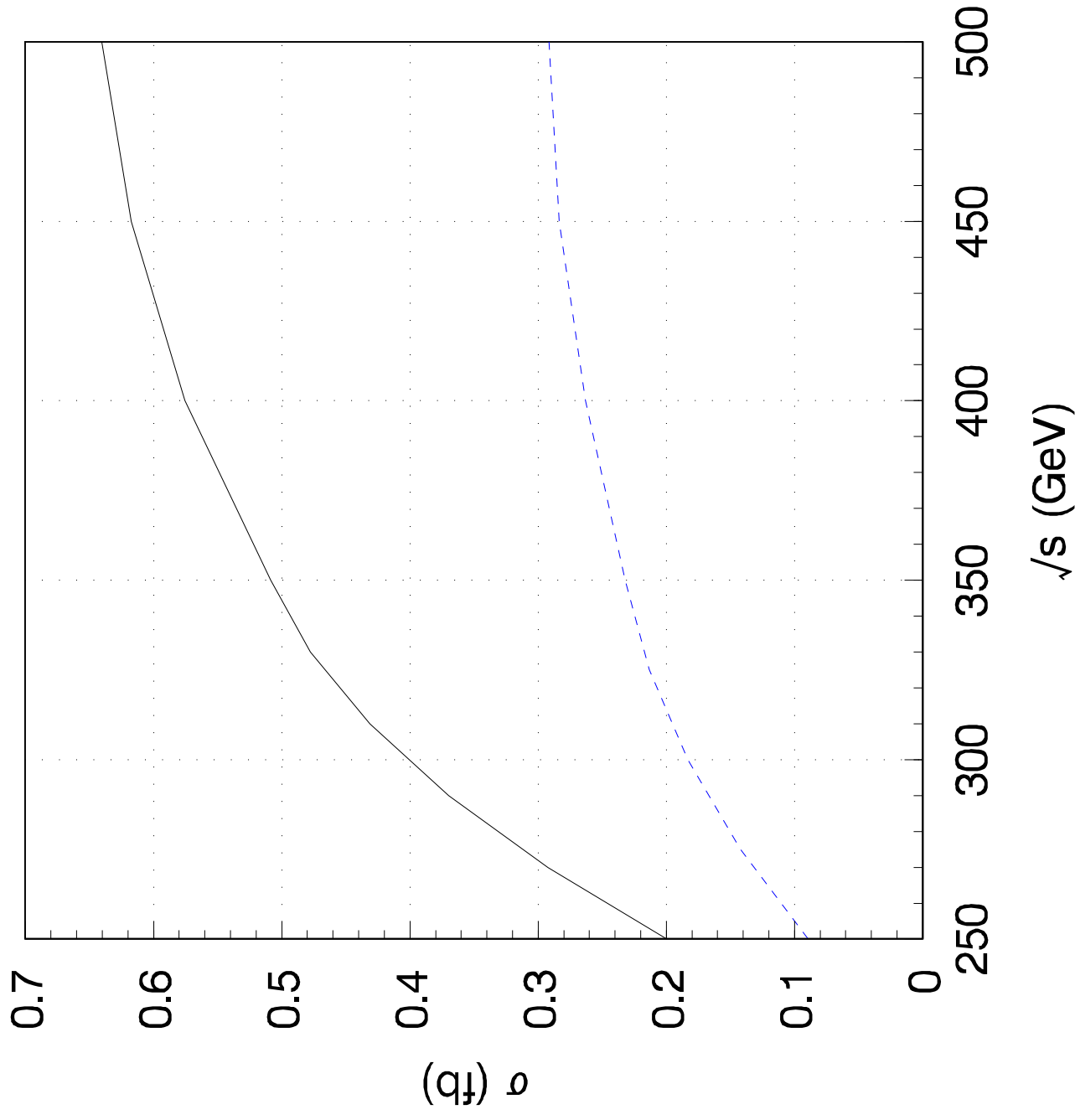


Fig.3

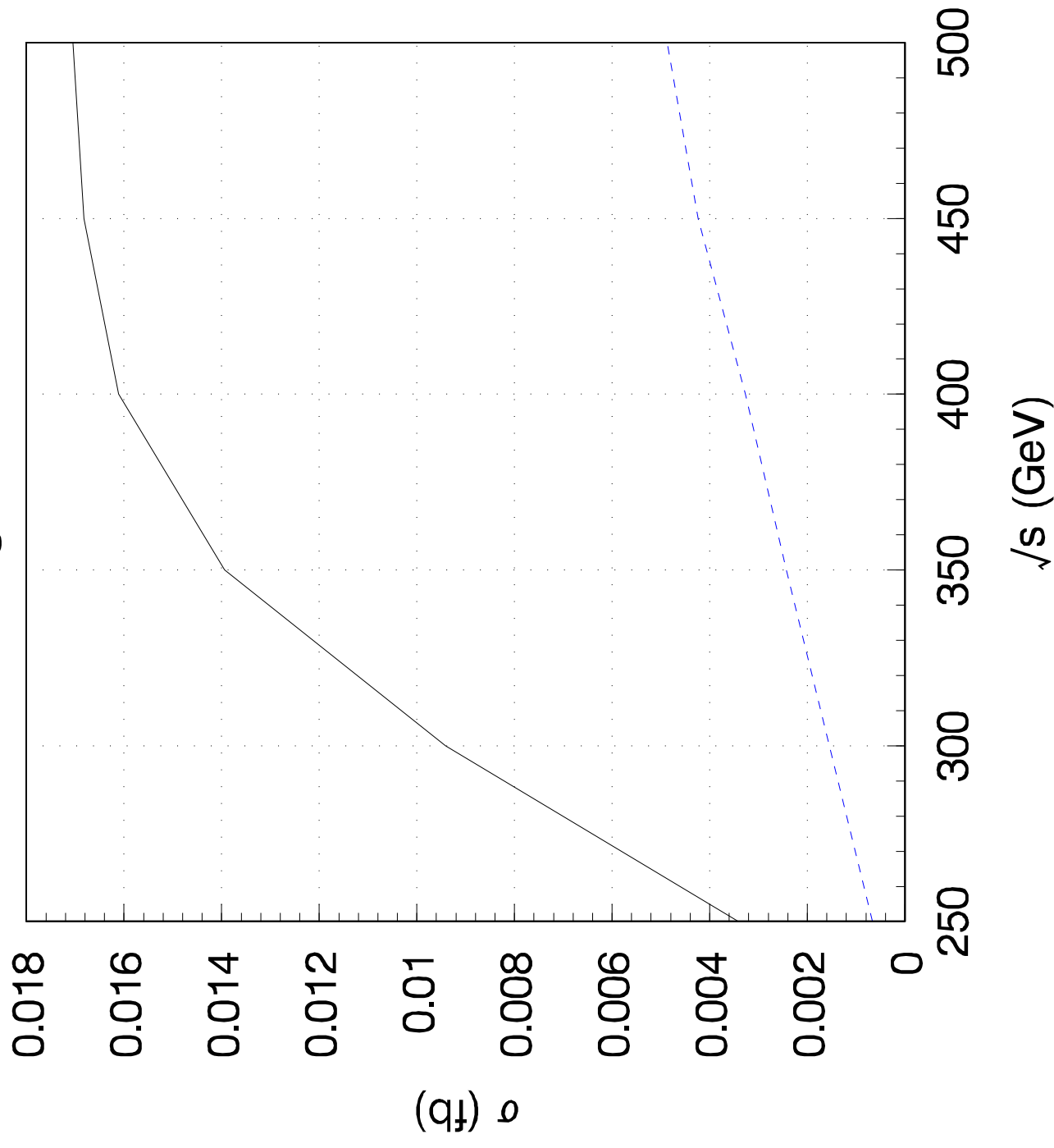


Fig.4

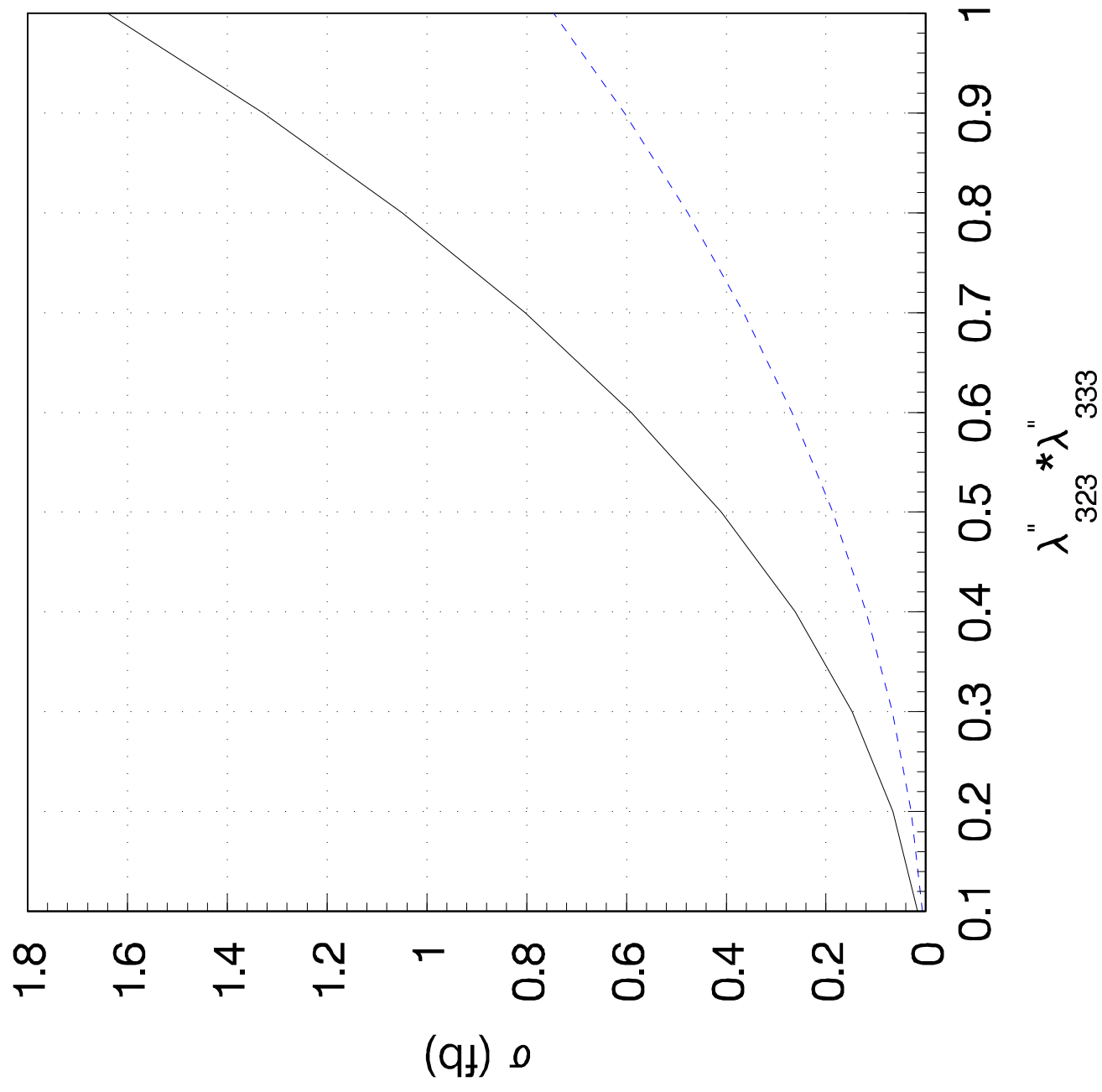


Fig.5

